medRxiv preprint doi: https://doi.org/10.1101/2024.02.01.24301979; this version posted February 3, 2024. The copyright holder for this preprint (which was not certified by peer review) is the author/funder, who has granted medRxiv a license to display the preprint in perpetuity. All rights reserved. No reuse allowed without permission.

White Matter Microstructure Alterations and Their Link to Symptomatology in Early Psychosis and Schizophrenia

Tommaso Pavan[1], Yasser Alemán-Gómez[1], Raoul Jenni[2], Pascal Steullet[2], Zoé Schilliger[2,6], Daniella Dwir[2], Martine Cleusix[2], Luis Alameda[3,4,5], Kim Q. Do[2], Philippe Conus[3], Paul Klauser[2,6], Patric Hagmann[1] and Ileana Jelescu[1]

1. Department of Radiology, Lausanne University Hospital (CHUV) and University of Lausanne (UNIL)
2. Center for Psychiatric Neuroscience, Department of Psychiatry, Lausanne University Hospital and the University of Lausanne, Lausanne Switzerland
3. Service of General Psychiatry, Treatment and Early Intervention in Psychosis Program. Lausanne University Hospital (CHUV), Lausanne, Switzerland
4. Department of Psychosis Studies, Institute of Psychiatry, Psychology and Neuroscience. King's College of London, London, UK.
5. Centro Investigacion Biomedica en Red de Salud Mental (CIBERSAM); Instituto de Biomedicina de Sevilla (IBIS), Hospital Universitario Virgen del Rocio, Departamento de Psiquiatria, Universidad de Sevilla, Sevilla, Spain.
6. Service of Child and Adolescent Psychiatry, Department of Psychiatry, Lausanne University Hospital and the University of Lausanne, Lausanne, Switzerland

Corresponding author: Tommaso Pavan; address: *Centre de Recherche en Radiologie*, PET3, CHUV, Rue du Bugnon 46, 1011, Lausanne, Switzerland ; telephone:+41213146020; fax:+41213146020; email: tommaso.pavan@chuv.ch

NOTE: This preprint reports new research that has not been certified by peer review and should not be used to guide clinical practice.

medRxiv preprint doi: https://doi.org/10.1101/2024.02.01.24301979; this version posted February 3, 2024. The copyright holder for this preprint (which was not certified by peer review) is the author/funder, who has granted medRxiv a license to display the preprint in perpetuity. All rights reserved. No reuse allowed without permission.

Abstract

Background and Hypothesis: Studies on schizophrenia feature diffusion magnetic resonance imaging (dMRI) to investigate white matter (WM) anomalies. The heterogeneity in the possible interpretations of these metrics highlights the importance of increasing their specificity. Here, we characterize WM pathology in early psychosis (EP) and schizophrenia (SZ) with increased specificity using advanced dMRI metrics: Diffusion Kurtosis Imaging and White Matter Track Integrity – Watson (WMTI-W) biophysical model. This enables us to better characterize WM abnormalities and relate them to the patient's symptomatology.

Study Design: dMRI-derived microstructure features were extracted from all of WM and from individual tracts in 275 individuals. 93 patients with EP and 47 with SZ were compared respectively to 135 age-range matched healthy controls (HC). The relationships between the dMRI metrics in WM and various clinical scales were investigated in each patient group.

Study Results: WM diffusivities were higher, while kurtosis was lower in EP and SZ vs HC. Differences were more pronounced in EP than SZ. WMTI-W model parameters suggest alterations to the extra-axonal compartment in EP and SZ, consistent with abnormal myelin integrity and WM deterioration. Patient groups showed clustered but non-significant correlations between dMRI metrics and psychotic symptoms. Depressive dimensions were significantly associated with decreased diffusivities in WM, while manic scales correlated with increased diffusivities and reduced kurtosis.

Conclusions: dMRI patterns in EP and SZ highly suggest WM deterioration in comparison to HC. DMRI changes better align with affective dimensions, while the relationship with psychotic symptoms may be confounded by competing pathological effects on the microstructure and disease heterogeneity.

medRxiv preprint doi: https://doi.org/10.1101/2024.02.01.24301979; this version posted February 3, 2024. The copyright holder for this preprint (which was not certified by peer review) is the author/funder, who has granted medRxiv a license to display the preprint in perpetuity. All rights reserved. No reuse allowed without permission.

Introduction

Positive and negative symptoms are the core characteristics for the diagnosis of schizophrenia (SZ) and other psychotic disorders. The former include delusions and hallucinations, and the latter encompass diminished emotional expression and avolition[1,2]. Nonetheless, an overlap between the clinical phenotypes of psychosis and mood disorders exists[3], leading to a subset of psychosis patients to suffer from mood disorder symptoms and vice versa. Many clinical studies used diffusion magnetic resonance imaging (dMRI) and reported pathological white matter (WM) as a common feature of the disturbances of the psychosis spectrum[4–11]. The great majority of these studies focus on Diffusion Tensor Imaging (DTI) and its scalar metrics: the most frequently reported and accepted dMRI patterns are reduced fractional anisotropy (FA) and increased mean diffusivity (MD) in patients with chronic SZ[4,6,7,10,12,13] and early psychosis[4,6–8,14–18] (EP), often reported widespread but with limited spatial consistency[4,5,10,19]. Such heterogeneity may arise not only from the patients themselves[19] but also from different pathological processes affecting the WM, with tracts showing non-degenerating early maturational shifts, or displaying accelerated aging[5]. Postmortem studies further substantiate the WM involvement found in first episode patients[20] and in SZ, reporting myelinated fiber pathology together with dystrophic oligodendroglia[21–24]and microglia[25].

Several relationships between psychopathological scores and dMRI measures have also been reported but remain unclear. Positive associations have been found between FA and positive symptoms[14,26,27], while FA and MD were inversely related to negative symptoms severity[7,26]. In contrast, other studies reported positive correlation between FA and negative symptoms in the corpus callosum[28] as well as anti-correlation between positive symptom and FA in the forceps minor[29]. Finally, one meta-analysis reported no significant association between symptoms and dMRI metrics[10].

Changes in FA and MD can be the consequence of several possible pathological mechanisms like edema[30], demyelination[31,32], axonal loss or their combination[33–35]. The heterogeneity in the possible interpretations highlights the importance of increasing the specificity of available in vivo dMRI-derived microstructure metrics by studying the radial and axial diffusivity estimates of DTI, which are rarely reported[4,5,9,15,27,36], and estimate Diffusion Kurtosis Imaging[37,38] (DKI), an extension of DTI. DKI provides complementary information about tissue heterogeneity at the mesoscale level by quantifying non-Gaussian diffusion arising from heterogeneous diffusion sub-domains within the voxel. DKI has been able to detect widespread WM abnormality[39] in regions with complex fiber arrangement[40], and subtle abnormalities in subjects at high risk for psychosis[41]. Nevertheless, DTI and DKI metrics are only *sensitive* to features of the tissue microstructure. To gain specificity, WM biophysical models of diffusion can be used[42]. Examples of biophysical model applications to EP and SZ are free-water imaging[43] (FWI) and Neurite Orientation Dispersion and Density Imaging[44] (NODDI). Most FWI studies reported a global increase in free-water (FW) in SZ[45] and across lifespan[46] (15–58 years). NODDI detected decreased neurite density (ND) and increased orientation dispersion index (ODI) in first episode[47,48] and in patients with SZ[49]. However, both models showed limitations in terms of *ad hoc* simplifying assumptions and fit constraints, strongly limiting the interpretability of the microstructure parameters estimated from the data[42,50].

In this work we use a more comprehensive biophysical model: White Matter Track Integrity-Watson[51–53] (WMTI-W, **Fig. 1**). WMTI-W features two non-exchanging compartments allowing the estimation of intra- and extra-axonal specific diffusivities that are excellent proxies for intra-axonal injury, inflammation and abnormal myelin integrity respectively[34,42,52]. WMTI and WMTI-W have been recently used to characterize WM pathology in a variety of patient populations[54,55] and animal models of disease[31,32], ranging from Alzheimer's disease[56–58] to traumatic brain injury[59], but never in schizophrenia. By employing a more comprehensive microstructure model in an exploratory fashion, we aim to characterize for the first time WM pathology in EP and SZ with increased specificity and thus relate it better to the observed symptomatology of our cohort. We hypothesize that this method will overcome the multiple inconsistencies previously found in SZ and in the relation between dMRI metrics and symptom domains.

Methods

Participants

The data used for this study was collected from 275 individuals and divided into three groups: 135 healthy controls (HC), 93 EP and 47 SZ (**Table 1**). EP patients (within 5 years after a first psychotic episode as defined by the Comprehensive Assessment of At-Risk Mental States scale[60], CAARMS) or SZ patients with a DSM-IV diagnosis of schizophrenia and schizoaffective disorder were recruited from the Lausanne University Hospital. EP patients with psychosis related to intoxication, organic brain disease, or IQ<70, were excluded, as well as SZ individuals reporting alcoholism, drug abuse, major somatic disease, documented anamnestic or current organic brain damage. Finally, HC

medRxiv preprint doi: https://doi.org/10.1101/2024.02.01.24301979; this version posted February 3, 2024. The copyright holder for this preprint (which was not certified by peer review) is the author/funder, who has granted medRxiv a license to display the preprint in perpetuity. All rights reserved. No reuse allowed without permission.

were excluded if they, or a first-degree family member, suffered from psychosis or prodromal symptoms, or reported current or past antipsychotic treatment. The HC group was further subdivided into younger (HC-Y, n=130, age=26.8±6.8) and older (HC-O, n=84, age=31.9±8.1) to better match the age ranges of the two clinical groups (EP=24.7±5.5; SZ=38.1±9.4 years). Participants provided written informed consents. The study was conducted in accordance with the Declaration of Helsinki and approved by the local Ethics Committee of the Canton of Vaud (Switzerland) under authorization numbers CER-VD 382/11 and 2018-01731. Within-group individual diagnoses are reported in **Supplementary Table S1.**

MRI acquisition

MRI scanning sessions were performed on two different 3-Tesla systems (Magnetom TrioTim and PRISMA, Siemens Healthineers, Erlangen, Germany), each equipped with a 32-channel head coil. A 1-mm isotropic T1-weighted image was acquired for anatomical reference. Whole-brain diffusion-weighted images (DWI) were acquired using diffusion spectrum imaging (DSI) scheme across 15 b-values, ranging from 0 to 8000 s/mm^2, voxel size of 2.2 x 2.2 x 3 mm^3. Further information can be found in the acquisition details section of the Supplementary Material.

Image preprocessing

The MPRAGE image was bias field corrected[61] and skull-stripped via nonlinear registration to the MNI-152 template[62] using Advanced Normalization Tools[63] (ANTs). The diffusion preprocessing pipeline included MP-PCA denoising, Gibbs ringing-, EPI-, eddy current and motion corrections, following most recent guidelines[64] - see Supplementary Material for preprocessing details.

Microstructure estimation

For DKI and WMTI-W estimation, the diffusion dataset was truncated at b≤2500 s/mm^2 (Jensen et al., 2005). DKI was fit voxel-wise in the entire brain[65] using Matlab, from which seven parameter maps were derived: four from DTI: radial, mean, axial diffusivity (RD, MD, AD) and fractional anisotropy (FA), and three from DKI: radial, mean, axial kurtosis (RK, MK, AK). Then, WMTI-W model parameters were estimated voxel-wise from the DTI and DKI parameters, using an in-house Python script, yielding other five parameter maps: axonal density f, intra-axonal diffusivity D_a, extra-axonal parallel and perpendicular diffusivities $D_{e,//}$, $D_{e,\perp}$ and axon orientation alignment c_2 (**Fig. 1**). The WM characterization thus relied on 12 microstructure metrics.

ROI analysis

Individual FA maps were non-linearly registered to the Johns Hopkins University FA template[66] (JHU) using ANTs, and the WM region-of-interest (ROI) labels from the template were then mapped back to individual space using the resulting spatial transformations. The mean value of each microstructure metric was computed inside each ROI and their ensemble (whole JHU-defined WM, from here on referred to as core of the WM).

Psychiatric scales

Level of functioning was assessed with the Global Assessment of Functioning[67] scale (GAF). Symptom levels were measured with the Positive and Negative Syndrome Scale[68] (PANSS), the Montgomery-Asberg Depression Rating Scale[69] (MADRS) and the Young Mania Rating Scale[70] (YMRS). For the PANSS, items were categorized using the Wallwork/Fortgang five-factor model[71] (WW) which comprises five dimensions: positive (pos.), negative (neg.), disorganized (dis.), depressive (depr.) and excited dimension (exc.). PANSS data was not available for 5 EP and 1 SZ subjects, MADRS and YMRS were not assessed in 6 EP and 16 SZ subjects.

Statistical analysis

Before any statistical analysis, all the microstructure parameter estimates in the WM core and individual JHU ROIs were harmonized for scanner type via ComBat harmonization[72] that has proven efficient at correcting scanner effects in the same cohort[73]. Distributions for each metric, ROI and group were tested for normality using the Shapiro–Wilk test[74] and for homogeneity of variance using the Levene's Test[75]. The statistical test used for group comparisons was chosen based on distribution characteristics, resulting in dMRI metrics for the WM core being tested via non-parametric Wilcoxon signed-rank[76] test, suitable for non-normal but homogeneous variance distributions. At the ROI level, dMRI metrics between groups were compared using the non-parametric Brunner-Munzel[77,78] test, suitable for distributions with unequal variances. In all comparisons, the estimates were controlled for sex and quadratic[5] age, and p-values were false discovery rate (FDR) corrected. The model selection procedure for age correction is reported in the age correction section of the supplementary material and plot in **Supplementary**

medRxiv preprint doi: https://doi.org/10.1101/2024.02.01.24301979; this version posted February 3, 2024. The copyright holder for this preprint (which was not certified by peer review) is the author/funder, who has granted medRxiv a license to display the preprint in perpetuity. All rights reserved. No reuse allowed without permission.

Figure S1. The dice coefficient was used to quantify the similarity in ROI alterations across the brain, indicating the proportion (between 0 and 1) of significant alterations that EP and SZ groups have in common.
Microstructure metrics in the WM core were correlated to psychiatric scales. The correlation matrices for EP and SZ were analyzed via hierarchical clustering (distance: *euclidean*; clustering method: *complete linkage*; *dist*, *hclust* functions in R[79]) and p-values were FDR-corrected. Finally, the individual correlations that remained significant were further investigated via robust regression (*robustbase*[80,81]), to ensure robustness to outliers, and a second correlation analysis was performed to determine which JHU ROIs contributed the most to the significant association in the whole WM core.

medRxiv preprint doi: https://doi.org/10.1101/2024.02.01.24301979; this version posted February 3, 2024. The copyright holder for this preprint (which was not certified by peer review) is the author/funder, who has granted medRxiv a license to display the preprint in perpetuity. All rights reserved. No reuse allowed without permission.

Results

Cohort demographics

The cohort demographics are displayed in **Table 1**. Significant differences were found in age between groups (p<.0001), leading to the inclusion of age as a covariate. Significant differences between EP and SZ were found in the illness duration (p<.0001) but not in the age at onset or CPZ-equivalent dose.

Diffusion kurtosis and microstructure imaging estimates

The estimated study templates for DTI, DKI and WMTI-W metrics are plotted in **Fig. S2**. The harmonized mean estimates of the WM core are reported for the four distinct groups in **Table S2**. In the WM core, several group differences were found (**Fig. 2**). Compared to HC-Y, EP showed significantly higher DTI diffusivities and lower FA (**Fig. 2A** to **D**; RD, MD: p<.0001, FA: p=.00021, AD: p=.018), as well as lower kurtosis (**Fig. 2E, F, G**; RK: p=.0035, MK: p=.0060; AK: p=.041). Axonal water fraction, f, and alignment, c_2, in EP were also significantly lower than in HC-Y (**Fig. 2H, L**; f: p=.013 c_2: p=.0022), while extra-axonal diffusivities, $D_{e,//}$ and $D_{e,\perp}$, were higher (**Fig. 2J, K**; $D_{e,//}$: p=.0022, $D_{e,\perp}$: p=.00011). No significant differences were found between EP and HC-Y in terms of intra-axonal diffusivity D_a (**Fig. 2I**). Differences between SZ and HC-O were more limited, with no differences at the level of DTI metrics. Kurtosis, however, was also lower in SZ (**Fig. 2E, F, G**; RK: p=.036, MK: p=.018, AK: p=.037). The WMTI-W metrics showing significant differences were reduced f (**Fig. 2H**; p=.036), increased D_a (**Fig. 3I**; p=.018) and $D_{e,//}$ (**Fig. 2J**, p=.036). Numeric p-values, effect sizes, and confidence intervals can be found in **Table S3**. We found no significant differences between EP and SZ (see **Table S4**).

Group comparison of the JHU ROIs revealed distinct patterns in the dMRI metrics tendencies, highlighting ROI specific alterations in both EP and SZ (**Fig. 3**). Most affected bundles included the corpus callosum (CC), fornix (FX), corona radiata (CR), posterior thalamic radiation (PTR), sagittal stratum (SAGSTR), cingulum (CING/CG) and superior longitudinal fasciculus (SLF).

Common features were higher DTI diffusivities in both EP and SZ with respect to their HC groups, with the EP group having the most distinct and widespread increase across the WM. We quantified the percentages of WM ROIs with higher RD, MD, and AD, respectively: 56, 54, 18% in EP and 12, 16, 8% in SZ (**Fig. 3**, both DTI sections, in red). These differences were generally paired to lower FA of the same ROI in EP, but not as consistently in SZ (34 vs 4%; **Fig. 3**, both blocks, FA in DTI sections).

Kurtosis metrics were lower in both patient groups (**Fig. 3**, both DKI sections, in blue). In EP, the significantly lower DKI metrics were matched to the changes in DTI metrics except for the bilateral cerebellar peduncle (CP) and CING (hippocampal section acc. JHU) areas. Decreased kurtosis was significant for RK, MK and AK in 24%, 34% and 20% of ROIs, respectively (**Fig. 3**, upper-block, DKI section, in blue). In SZ patients, this trend was notably less consistent (RK: 20%, MK: 24%, AK: 12% of ROIs; **Fig. 3**, bottom-block, DKI section, in blue), with some ROIs showing alterations detected by DKI and not DTI, such as the bilateral SAGSTR, the left anterior limb of internal capsule (ALIC) and FX and vice versa, e.g. in CING and right anterior corona radiata (ACR). WMTI-W metrics display the same trends as for the whole WM analysis, with f lower in several locations of the WM in SZ and especially EP (10% vs 18% of ROIs, **Fig. 3**, WMTI sections, in blue), and higher extra-axonal diffusivities. In EP, $D_{e,//}$ and $D_{e,\perp}$ were significantly altered in 24 and 20% of the ROIs respectively. In the SZ group, $D_{e,//}$ and $D_{e,\perp}$ showed fewer number of significant alterations, 16% and 6%. Notably, D_a alterations were uncommon in both groups and not spatially consistent. Finally, sparse c_2 alterations were found in EP (6% of ROIs) but none in SZ (**Fig. 3**, both blocks, WMTI section, in red). Overall, the Dice coefficient between EP and SZ differences to their respective HC (heatmaps) was 0.36, measuring the agreement across altered ROIs. For additional details about FDR p-values, effect size and confidence intervals see **Table S5** and **Table S6**.

Association between microstructure estimates and psychopathological symptom domains

Differences in psychiatric scales between EP and SZ can be found in **Table 1**. We correlated psychiatric scores to microstructure metrics in the whole WM core because dMRI metrics showed consistent changes across JHU ROIs and this approach limited the number of statistical tests.

Overall, correlations between psychiatric scales and dMRI metrics in WM were stronger in SZ than EP (**Fig. 4A** vs **B**). In both groups, hierarchical clustering identified three macro clusters in dMRI metrics (**Fig. 4A, B** top dendrograms and vertical columns): i) diffusivities (RD, MD, AD, $D_{e,//}$, $D_{e,\perp}$, D_a), ii) variance within voxels informing about the tissue complexity (RK, AK, MK, f), and iii) axonal bundle anisotropy (FA, c_2).

The clustering of psychiatric dimensions revealed patterns of correlation between dMRI metrics and psychiatric scales within the clinical groups, particularly in SZ. In EP, psychiatric dimensions were classified into three clusters

medRxiv preprint doi: https://doi.org/10.1101/2024.02.01.24301979; this version posted February 3, 2024. The copyright holder for this preprint (which was not certified by peer review) is the author/funder, who has granted medRxiv a license to display the preprint in perpetuity. All rights reserved. No reuse allowed without permission.

(**Fig. 4A**, Dimensions, left dendrogram). The first cluster, which included GAF, WW neg. and WW dis., showed weak pattern of correlations with dMRI metrics. The second cluster, which included WW pos. and YMRS, (**Fig. 4A**), showed a selective positive association with the WM complexity metrics and weak negative correlations with the tissue diffusivities. The third cluster, which grouped affective symptoms (WW exc., WW depr. and MADRS) was characterized by negative associations with the tissue diffusivities and positive with complexity metrics (**Fig. 4A**). However, only the correlations of lower MD and RD with higher WW depr. score, were significant after FDR correction.

In SZ, the clustering of the symptom dimensions differed from that of EP (**Fig. 4B**). A first cluster was found for manic behaviors, where YMRS and WW exc. scores correlated with increased dispersion (lower FA, c_2), increased diffusivities, and decreased complexity metrics (**Fig. 4B**, first cluster), opposite of EP trends for the same dimensions. YMRS correlations to FA, c_2, MD, RD, and $D_{e,\parallel}$ remained significant after FDR correction. A second cluster comprising WW neg., pos., and dis. was characterized by negative associations with anisotropy metrics (FA, c_2), and positive associations with complexity metrics. In this cluster, WW dis. showed stronger association to kurtosis, f and c_2 than WW neg and pos. Finally, the third cluster which included depressive symptoms (WW depr. and MADRS) and GAF, primarily shared a consistent negative correlation with complexity metrics (**Fig. 4B**). Notably, the axonal anisotropy metrics, FA and c_2, were the measures that showed the most consistent correlations among the symptom dimensions in SZ.

To further analyze the correlations between dMRI metrics and psychiatric scales, we plotted those correlations that survived multiple comparison correction (identified by an asterisk in **Fig. 4A, B**). Robust regression analysis yielded correlation coefficients of r=-.26 (p=.015) and r=-.24 (p=.037), between the WW depressed factor and AD and MD, respectively, in EP (**Fig. S3A, B**). The ROI-wise correlation analysis revealed that the body of the corpus callosum (BCC), right superior CP, superior CR, and right cingulum (CING) were the ROIs mostly driving these significant associations (**Fig. S6A**).

In SZ, YMRS total (**Fig. 4B**) score was the dimension which significantly correlated with the highest number of dMRI metrics. These metrics were MD (r=.47, p=.0012; **Fig. S5A**), RD (r=.55, p=.0015; **Fig. S5B**), $D_{e,\parallel}$, (r=.60, p=.0059; Fig. **S5D**), FA (r=-.60, p=.0024; **Fig. S5C**) and the axonal orientation alignment c_2 (r=-.66, p=.017; **Fig. S5E**). However, we could not find a subgroup or specific YMRS items that could unambiguously explain these findings and, overall, SZ patients in our cohort did not score beyond the YMRS remission threshold (YMRS total score ≤12). To try to further understand our findings, we tested the individual items defining the WW exc. (PANSS P4-excitement, P7-hostility, G8-uncooperativeness and G14-impulse control[71]), which was clustered with the YMRS scale. We found that only the P4-excitement item significantly correlated (after FDR correction) to RD (r=.41, p=.012), MD (r=.38, p=.020), FA (r=-.40, p=.013) and $D_{e,\parallel}$ (r=.40,p=.012. The ROI-wise correlation analysis revealed widespread associations of the YMRS scores across the WM (**Fig. S6B**), including CC, sections of the bilateral CP, bilateral ALIC, the entirety of the CR, PTR, SAGSTR, left EC, fornix/stria (FX/STRIA), superior and inferior fronto-occipital fasciculus (SFOF, IFOF) and uncinate fasciculus (UF). Finally, the significant negative association between the WW disorganized factor and c_2 in SZ (r=-.56, p=.023) is plotted in **Fig. S4**. In a similar fashion to the YMRS, the JHU ROI c_2 associations with the WW dis. factor were numerous, affecting bilaterally the CP, the ACR and the EC (**Fig. S6B**).

medRxiv preprint doi: https://doi.org/10.1101/2024.02.01.24301979; this version posted February 3, 2024. The copyright holder for this preprint (which was not certified by peer review) is the author/funder, who has granted medRxiv a license to display the preprint in perpetuity. All rights reserved. No reuse allowed without permission.

Discussion

With the present analysis we employed more advanced diffusion metrics than DTI, namely DKI and a comprehensive microstructure model, WMTI-W, both aimed at characterizing the WM pathology with increased sensitivity and specificity in our early psychosis and schizophrenia cohorts.

Our findings reveal that WM alterations as assessed using dMRI microstructure metrics are already present and widespread in the EP stage and differences in microstructure are less pronounced between chronic SZ and HC-O when accounting for age. Furthermore, most EP and SZ WM differences to HC concern the radial direction of diffusion, i.e., perpendicularly to the bundle main axis. Thus, RD and MD were the most affected, while AD differences were less significant. Our study confirms previous DTI[5,15,16,82], dMRI microstructure[73,83] and post-mortem cytoarchitectural[20] alterations found already at the EP stage, and the widespread reduced FA and increased MD[4–8,12,14–16,18,48], RD and AD[8,13,84,85] in areas commonly reported in EP and chronic SZ.

In addition, WM kurtosis was lower for both patient groups, but also more pronounced in EP, and more particularly in the radial direction (RK: 24% vs 20%, AK: 20% vs 12% of ROIs), representing a decrease in tissue complexity and heterogeneity[34,37,38,86]. Remarkably, in SZ vs HC-O, DKI was able to identify differences in WM ROIs (SAGSTR, left ALIC and FX) that were not evident in DTI. In a review from Pasternak et al.[87], all studies but one also reported reduced MK, with one study also reporting lower RK and AK in SZ patients[40].

Our ROI-specific differences in dMRI metrics between patients and controls were consistent with literature, as previous studies also reported alterations in CING[5], FX[88,89], CR[90–92], PTR[92,93] and SAGSTR[93] in EP, that remained present in SZ patients. CC and SLF[5,7] are considered to have a declining trajectory with aging in SZ[5,7] (either FA decrease or MD increase when compared to HC), but our results confirm only the SLF trajectory (increased MD, decreased FA in EP and decreased kurtosis in SZ), while the CC was not altered as much in SZ as in EP[5,88–93].

For the first time, we used WMTI-W, a comprehensive biophysical model of WM, to tease apart possible pathological contributions to the reported WM differences. In EP, WMTI-W helps attribute the observed alterations to the extra-axonal compartment, due to the significant increase in $D_{e,//}$ and $D_{e,\perp}$, but not D_a. The lower axonal water fraction f and orientation coherence c_2 are further consistent with pathological features such as reduced myelination and axonal density. The former have indeed been shown to induce an increase in $D_{e,\perp}$ and decrease in f (e.g. in mouse model of cuprizone demyelination[31,32]) while the increase in $D_{e,//}$ can be a consequence of overall reduced cellular density and thereby hindrance in the extra-axonal space. The SZ group was overall characterized by higher $D_{e,//}$ and lower f, also pointing to less densely packed extra-cellular space. The WM core analysis suggested also higher intra-axonal diffusivity D_a in this group, but only two specific ROIs sustained this trend (CING and CC). Previous works using NODDI[44], a comparable but more constrained biophysical model, also reported reduced neurite density (ND, comparable to f) in several ROIs and increased orientation dispersion index (ODI, corresponding to lower c_2) in both first episode and chronic patients[83]. These patterns of preferentially altered extra-axonal environment are also consistent with reports of global increase in "free water" using the FWI technique in SZ cohorts[45], although FWI conflates potential pathological mechanisms by defining a tissue compartment (intra- and extra-axonal) vs a free water (cerebral spinal fluid) one.

Pathological WM changes identified using WMTI-W are further supported by neuroimaging findings beyond dMRI, such as a 14% reduction in WM volume[94], and ultrastructural post-mortem studies reporting myelinated WM fiber pathology, mainly consequence of the decompacting and splitting of the myelin sheath, but also the inclusions of vacuoles in between myelin layers, small-axons atrophy, and the presence of swollen or dystrophic oligodendroglia[22–24] and microglia[25]. In parallel to these morphological changes, a 27-28% reduction in oligodendrocyte densities were reported in cortical layer III and subcortical areas[21] of SZ brains. Despite these histological analyses focused on the frontal brain regions[21–23,25] and on older patients and the postmortem nature of the examination, the pathological WM changes they report agree with changes evidenced by the whole-brain dMRI analysis and by the WMTI-W model microstructure parameters in the present study. Going forward, dMRI combined with careful biophysical modeling could continue to provide crucial information about cellular-level brain changes in EP and SZ in vivo and longitudinally.

The clustering of behavioral scales in the regression analysis with dMRI metrics revealed that most correlations between WM microstructure and symptomatology were weak and non-significant. Second, the affective dimensions correlated better with changes in WM microstructure, and these associations were more significant in the SZ cohort. Third, a set of within-group associations were in contrast with the microstructure group comparisons to age range-matched HC. Namely, opposite to the higher diffusivities, reduced kurtosis and reduced f found between SZ and HC, the cluster containing WW neg.-pos.-dis. showed a positive score association with complexity metrics (kurtosis, f) in SZ. A similar associative pattern was found in EP for the WW pos.-YMRS and WW depr.-exc.-MADRS clusters, that showed respectively a positive score association with complexity metrics (kurtosis, f), and a negative score association with diffusivities. Thus, worse symptoms on some of these scales within a given patient group were

medRxiv preprint doi: https://doi.org/10.1101/2024.02.01.24301979; this version posted February 3, 2024. The copyright holder for this preprint (which was not certified by peer review) is the author/funder, who has granted medRxiv a license to display the preprint in perpetuity. All rights reserved. No reuse allowed without permission.

mirrored by WM changes opposite of those found from the comparison to HC. This scenario could be caused by either the patient heterogeneity, especially in the EP group, or competing pathological mechanisms of deterioration[5]-abnormal myelination[31] vs neuroinflammation[34] that have opposite effects on dMRI metrics and, when combined, result in a more challenging interpretation. Indeed, neuroinflammation has the effect of reducing diffusivities and increasing kurtosis due to higher cellular crowding associated with microgliosis and astrocytosis[31,32,34,35]. In support of this mechanism, proinflammatory cytokines have been reported to be elevated in EP[95] and SZ[96], and related to negative symptoms in EP[95].

However, when examining closely the correlation of stronger depressive symptoms to lower MD and AD in EP, patients with low scores on these scales displayed elevated diffusivities compared to the HC-Y mean, consistent with EP to HC-Y group differences, while patients with high depressive scores displayed similar WM diffusivities to HC-Y. These results are consistent with reports that higher depressive dimensional scores were sometimes associated to fewer hospitalizations and fewer relapses at 3 and 5 years[97], indicating better outcome for these patients, although poorer prognosis was also often reported[98]. Furthermore, the ROIs driving this correlation (CC, CR, CING) are often highlighted in WM DTI studies of depression[99].

In SZ, a worse WW dis. score was found associated to worse fiber coherence, consistent with the group comparison results. Furthermore, lower score patients displayed c_2 values like those of HC-O, which diverged as the score increased. In the literature about SZ, disorganized symptoms have been related to decreased FA in the ACR[91] and cingulum[100] (similar to our findings), increased MD of the longitudinal fasciculus[7] and worse cognitive impairment[101].

Finally, when considering excitement and manic behavior, worse scores within the SZ group correlated with the signature of deteriorated WM, i.e., increased diffusivities, reduced kurtosis and were thus consistent with the SZ to HC-O group differences. The YMRS total score was found to be significantly associated with higher diffusivities and lower anisotropy, but also decreased complexity metrics, attributed to higher excitement symptoms, and diverging from HC-O as the score worsened. In the literature, findings have reported that the worsening of the disease was associated with impulsivity, aggression[22,102,103] and, in EP, higher excitement scores led to poorer prognosis[97]. Among the many ROIs contributing to these results, the most consistent were localized in the frontal regions (GCC, ALIC, ACR, UF), possibly related to the reported abnormal frontal activity associated with excitement symptoms in patients with SZ[104].

The first limitation of the present study is the heterogeneity of the patient cohorts, which may explain the weak relationships between the symptomatology and WM integrity. Thus, the generalizability of our conclusions needs to be confirmed in other cohorts. Furthermore, as symptoms are transitory in nature, the patient's symptomatic state at the time of the MRI scan or evaluation may differ from the state that led to the assigned clinical score. This mismatch highlights the challenges of relating brain pathology characterized non-invasively using dMRI to symptomatology and the necessity to embrace different approaches to face such heterogeneity.

In conclusion, with this work we demonstrated that WM alterations, already present at the early psychosis stages, manifest preferentially perpendicularly to the axons as major extra-cellular increase in diffusivities, reduced restricted water, decreased intra-cellular water fraction, and loss of fiber alignment. With time, these changes become less dramatic in chronic SZ as compared to age-matched controls. Finally, the current study is one of the few that reports relationships between symptoms and advanced dMRI brain WM microstructure. At the SZ stage, WM deterioration is linked to stronger excitement and manic scores.

Acknowledgments

This work was supported by the Swiss National Science Foundation (PCEFP2_194260, to I.J.), the National Center of Competence in Research (NCCR) "SYNAPSY - The Synaptic Bases of Mental Diseases" from the Swiss National Science Foundation (n° 51NF40 – 185897 to KQD & PC) and the Foundation Alamaya. Dr Alameda is supported by Carigest fellowship and by Frutiger Adrian et Simone fellowship. Dr Dwir is supported by Frutiger Adrian et Simone fellowship. The authors have nothing to disclose and there are no conflicts of interest.

medRxiv preprint doi: https://doi.org/10.1101/2024.02.01.24301979; this version posted February 3, 2024. The copyright holder for this preprint (which was not certified by peer review) is the author/funder, who has granted medRxiv a license to display the preprint in perpetuity. All rights reserved. No reuse allowed without permission.

Figures and Tables

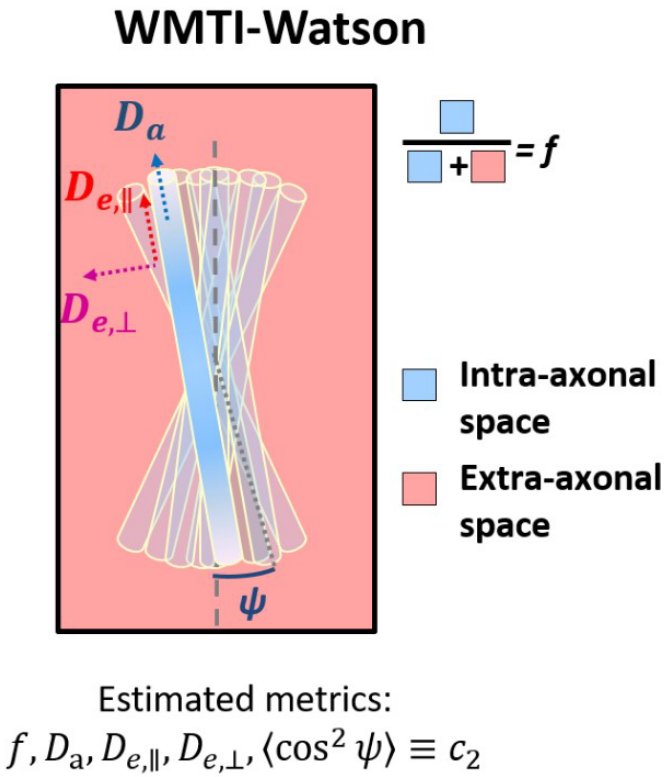

Figure 1 Schematics of White Matter Track integrity-Watson (WMTI-W) biophysical model. WMTI-W mimics the white matter environment by modelling axons as a collection of sticks. It estimates per voxel: the axonal water fraction f, the intra-axonal diffusivity, D_a, the extra-axonal parallel and radial diffusivities, $D_{e,//}$ and $D_{e,\perp}$, and the axonal orientation alignment, c_2. The extra-axonal compartment is modelled by $D_{e,//}$ and $D_{e,\perp}$ and describes the external diffusivities with respect to the main orientation of the axonal bundle. The intra-axonal compartment is modelled as a collection of impermeable zero-radius cylinders, mimicking the WM axons fascicles (*sticks*), and characterized by the remaining metrics. f measures the proportion of water in the voxel accounted for the WM axons. D_a represents the diffusivity within the axons. While c_2 quantify how aligned are the axons and it is derived from the concentration parameter of the Watson distribution, k. k is converted to c_2 to simplify its interpretation, following: $c_2 \approx \langle cos^2\psi \rangle$, with ψ being the angle between axons and the main bundle orientation. c_2 varies between 0, isotropic, and 1, perfectly parallel axons.

medRxiv preprint doi: https://doi.org/10.1101/2024.02.01.24301979; this version posted February 3, 2024. The copyright holder for this preprint (which was not certified by peer review) is the author/funder, who has granted medRxiv a license to display the preprint in perpetuity. All rights reserved. No reuse allowed without permission.

		HC-Y (N=130)		HC-O (N=84)		EP (N=93)		SZ (N=47)		EP-(HC-Y)	SZ-(HC-O)	EP-SZ
		Mean	SD	Mean	SD	Mean	SD	Mean	SD	p-value	p-value	p-value
Age (years)		26.8	6.8	31.9	8.1	24.7	5.5	38.1	9.4	3.0e-02*	5.6e-05****	p=3.5e-15****
Age at Psychosis Onset (years)						23.0	5.8	23.8	9.3			ns
Duration of illness (months)						16.3	15.5	160.8	77.9			p=1.3e-18****
CPZ-equivalent dose (mg/day)						341.0	274.5	319.6	287.7			ns
Delta MRI-Clin. Ass. (months)		2.5	5.5	3.1	6.9	2.1	3.2	6.6	21.3			p=1.0e-03**
PANSS: total						62.7	15.6	62.0	15.9			ns
PANSS: positive symptoms						12.9	4.1	14.3	4.8			ns
PANSS: negative symptoms						16.5	5.9	16.2	5.7			ns
PANSS: general psychopathology						33.2	8.6	31.8	8.8			ns
PANSS-WW: positive						7.0	2.9	8.3	3.6			p=2.3e-02*
PANSS-WW: negative						14.9	5.7	14.0	5.4			ns
PANSS-WW: disorganized						5.7	2.2	6.5	2.2			p=2.8e-02*
PANSS-WW: excited						6.1	2.2	6.2	2.1			ns
PANSS-WW: depressed						8.2	2.8	8.1	3.3			ns
GAF		83.9	4.4	83.4	4.7	56.2	11.2	56.0	13.2	1.6e-33****	4.6e-16****	ns
MADRS tot.						12.5	8.4	13.2	8.6			ns
YMRS tot.						3.2	4.1	3.8	3.9			ns
		N	Pct.%	N	Pct.	N	Pct.%	N	Pct.%			
Scanner	Prisma	67	51.5	43	51.2	59	63.4	20	42.6	χ^2:6.3	p=.096 ns	
	Trio	63	48.5	41	48.8	34	36.6	27	57.4			
Sex	Female	46	35.4	35	41.7	26	28.0	13	27.7	χ^2:4.67	p=.19 ns	
	Male	84	64.6	49	58.3	67	72.0	34	72.3			

Table 1 Cohort demographics. HC amount to 135 Individual, 79 HC were shared between HC-Y and HC-O. P-values refer to Wilcox's tests between clinical and healthy control groups. χ^2 test is computed for the whole scanner and sex contingency table. HC: healthy controls, Y: young, O: old, EP: early psychosis, SZ: chronic schizophrenic, Delta MRI-Clin. Ass.: difference in months between MRI scan and clinical assessment, SOFAS: Social and Occupational Functioning Assessment Scale, GAF: Global Assessment of Functioning, PANSS: Positive and Negative Syndrome Scale, MADRS: Montgomery-Asberg Depression Rating Scale, YMRS the Young Mania Rating Scale.

medRxiv preprint doi: https://doi.org/10.1101/2024.02.01.24301979; this version posted February 3, 2024. The copyright holder for this preprint (which was not certified by peer review) is the author/funder, who has granted medRxiv a license to display the preprint in perpetuity. All rights reserved. No reuse allowed without permission.

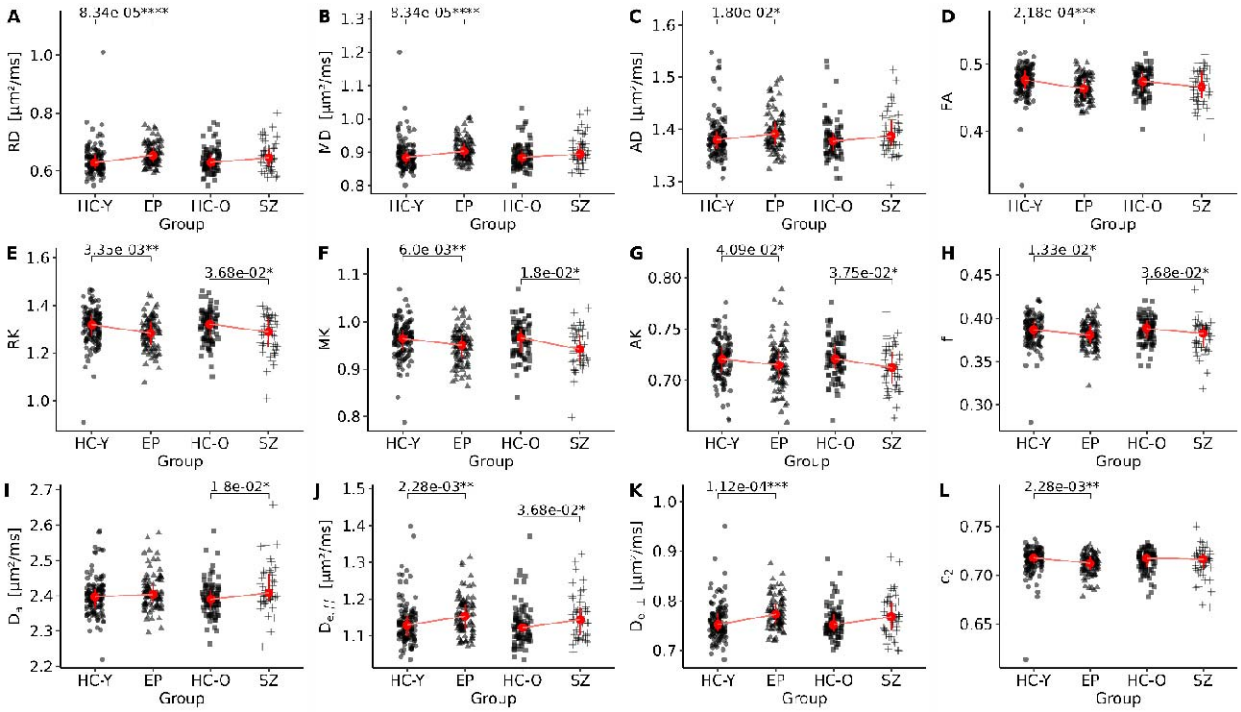

Figure 2 Strip plot of the group comparisons. Each clinical group is compared to its respective HC group. EP: early psychosis, SZ: chronic schizophrenic, HC-Y/O: healthy controls young/old. *:p≤5e-2, **:p≤1e-2, ***:p≤1e-3, ****:p≤1e-4.

medRxiv preprint doi: https://doi.org/10.1101/2024.02.01.24301979; this version posted February 3, 2024. The copyright holder for this preprint (which was not certified by peer review) is the author/funder, who has granted medRxiv a license to display the preprint in perpetuity. All rights reserved. No reuse allowed without permission.

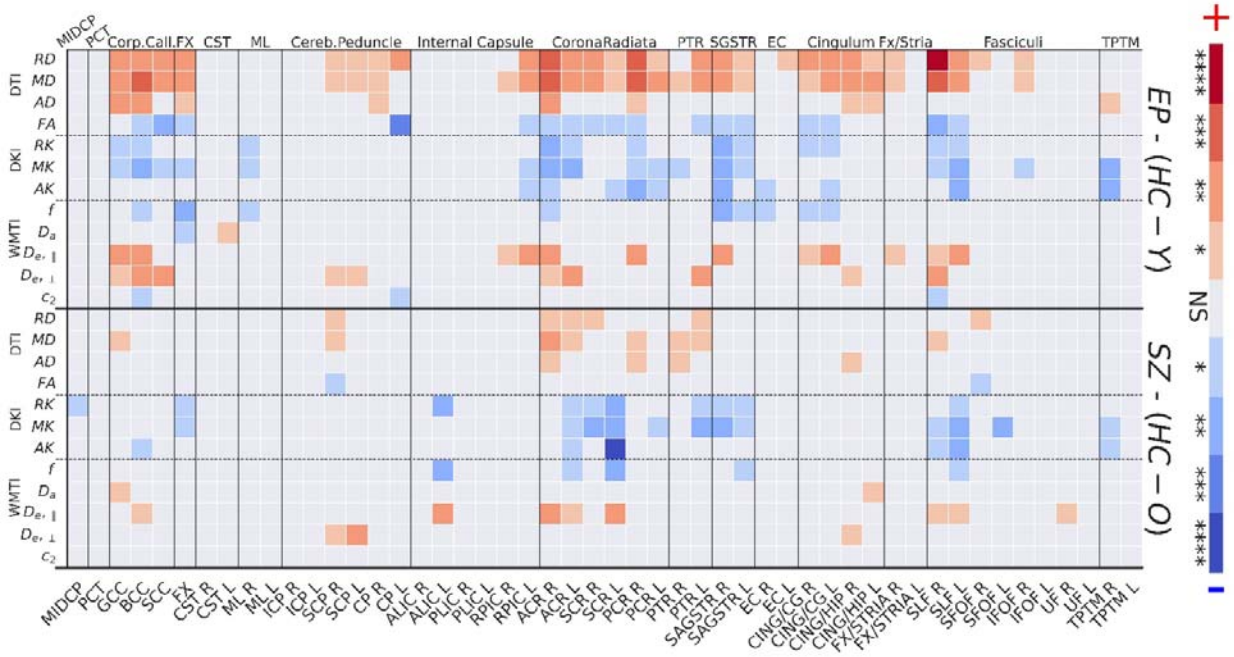

Figure 3 Heatmap of the ROI group comparison. Group comparisons (y-axis right) heatmap of the Brunner-Munzel test significance levels for each dMRI metric (y-axis left) and each region of interest (x-axis). Red: clinical group has higher value than the HC, Blue indicates the opposites. The darker the color, the lower is the p-value; ns: p≤1, *:p≤5e-2, **:p≤1e-2, ***:p≤1e-3, ****:p≤1e-4.

Abbreviations: EP: early psychosis; HC-Y/O: younger/older healthy control; SZ: chronic schizophrenia; L: left; R: right; MIDCP: Middle cerebellar peduncle; PCT: Pontine crossing tract (a part of MC; GCC: Genu of corpus callosum; BCC: Body of corpus callosum; SCC: Splenium of corpus callosum; FX: Fornix (column and body of fornix; CST: Corticospinal tract; ML: Medial lemniscus; ICP: Inferior cerebellar peduncle; SCP: Superior cerebellar peduncle; CP: Cerebral peduncle; ALIC: Anterior limb of internal capsule; PLIC: Posterior limb of internal capsule; RPIC: Retrolenticular part of internal capsule; ACR: Anterior corona radiata; SCR: Superior corona radiata; PCR: Posterior corona radiata; PTR: Posterior thalamic radiation (include optic radiation); SAGSTR: Sagittal stratum; EC: External capsule; CING/CG: Cingulum (cingulate gyrus); CING/HIP: Cingulum (hippocampus); FX/STRIA: Fornix (cres) / Stria terminalis ; SLF: Superior longitudinal fasciculus; SFOF: Superior fronto-occipital fasciculus; IFOF: Inferior fronto-occipital fasciculus; UF: Uncinate fasciculus; TPTM: Tapetum.

medRxiv preprint doi: https://doi.org/10.1101/2024.02.01.24301979; this version posted February 3, 2024. The copyright holder for this preprint (which was not certified by peer review) is the author/funder, who has granted medRxiv a license to display the preprint in perpetuity. All rights reserved. No reuse allowed without permission.

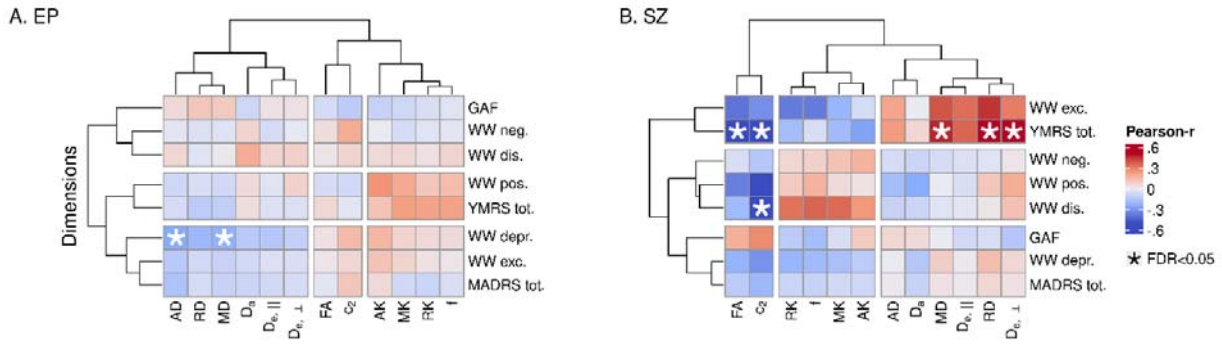

Figure 4 Hierarchical clustering of the correlation matrices between white matter microstructure estimates and psychopathological symptoms domains. The plot is divided into EP (A, left) and SZ (B, right) groups. Colors mark the Pearson correlation coefficient value (intensity) and positive (red) or negative (blue) direction of the association. The smaller cluster subdivisions indicate clusters of interests. Asterisks indicate those correlations whose FDR-corrected p-value is significant (FDR<.05). GAF: Global Assessment of Functioning scale; MADRS: Montgomery-Asberg Depression Rating Scale; YNRS: Young Mania Rating Scale; WW: Wallwork five-factor model for the Positive and Negative Syndrome Scale; pos.: positive; neg.: negative (neg.), dis.: disorganized; depr.: depressive; exc.: excited/manic dimension.

medRxiv preprint doi: https://doi.org/10.1101/2024.02.01.24301979; this version posted February 3, 2024. The copyright holder for this preprint (which was not certified by peer review) is the author/funder, who has granted medRxiv a license to display the preprint in perpetuity. All rights reserved. No reuse allowed without permission.

References

1. American Psychiatric Association. *Diagnostic and Statistical Manual of Mental Disorders*. Fifth Edition. American Psychiatric Association; 2013. doi:10.1176/appi.books.9780890425596

2. McCutcheon RA, Reis Marques T, Howes OD. Schizophrenia—An Overview. *JAMA Psychiatry*. 2020;77(2):201-210. doi:10.1001/jamapsychiatry.2019.3360

3. Kempf L, Hussain N, Potash JB. Mood disorder with psychotic features, schizoaffective disorder, and schizophrenia with mood features: Trouble at the borders. *Int Rev Psychiatry*. 2005;17(1):9-19. doi:10.1080/09540260500064959

4. Dwork AJ, Mancevski B, Rosoklija G. White matter and cognitive function in schizophrenia. *Int J Neuropsychopharmacol*. 2007;10(04):513. doi:10.1017/S1461145707007638

5. Cetin-Karayumak S, Di Biase MA, Chunga N, Reid B, Somes N, Lyall AE, et al. White matter abnormalities across the lifespan of schizophrenia: a harmonized multi-site diffusion MRI study. *Mol Psychiatry*. 2020;25(12):3208-3219. doi:10.1038/s41380-019-0509-y

6. Friedman Joseph I, Tang C, Carpenter D, Buchsbaum M, Schmeidler J, Flanagan L, et al. Diffusion Tensor Imaging Findings in First-Episode and Chronic Schizophrenia Patients. *Am J Psychiatry*. 2008;165(8):1024-1032. doi:10.1176/appi.ajp.2008.07101640

7. Waszczuk K, Tyburski E, Rek-Owodziń K, Plichta P, Rudkowski K, Podwalski P, et al. Relationship between White Matter Alterations and Pathophysiological Symptoms in Patients with Ultra-High Risk of Psychosis, First-Episode, and Chronic Schizophrenia. *Brain Sci*. 2022;12(3):354. doi:10.3390/brainsci12030354

8. Barth C, Kelly S, Nerland S, Jahanshad N, Alloza C, Ambrogi S, et al. In vivo white matter microstructure in adolescents with early-onset psychosis: a multi-site mega-analysis. *Mol Psychiatry*. 2023;28(3):1159-1169. doi:10.1038/s41380-022-01901-3

9. Karlsgodt KH. White Matter Microstructure across the Psychosis Spectrum. *Trends Neurosci*. 2020;43(6):406-416. doi:10.1016/j.tins.2020.03.014

10. Kelly S, Jahanshad N, Zalesky A, Kochunov P, Agartz I, Alloza C, et al. Widespread white matter microstructural differences in schizophrenia across 4322 individuals: results from the ENIGMA Schizophrenia DTI Working Group. *Mol Psychiatry*. 2018;23(5):1261-1269. doi:10.1038/mp.2017.170

11. van Velzen LS, Kelly S, Isaev D, Aleman A, Aftanas LI, Bauer J, et al. White matter disturbances in major depressive disorder: a coordinated analysis across 20 international cohorts in the ENIGMA MDD working group. *Mol Psychiatry*. 2020;25(7):1511-1525. doi:10.1038/s41380-019-0477-2

12. Pasternak O, Westin CF, Dahlben B, Bouix S, Kubicki M. The extent of diffusion MRI markers of neuroinflammation and white matter deterioration in chronic schizophrenia. *Schizophr Res*. 2015;161(1):113-118. doi:10.1016/j.schres.2014.07.031

13. Klauser P, Baker ST, Cropley VL, Bousman C, Fornito A, Cocchi L, et al. White Matter Disruptions in Schizophrenia Are Spatially Widespread and Topologically Converge on Brain Network Hubs. *Schizophr Bull*. 2017;43(2):425-435. doi:10.1093/schbul/sbw100

14. Cheung V, Chiu CPY, Law CW, Cheung C, Hui CLM, Chan KKS, et al. Positive symptoms and white matter microstructure in never-medicated first episode schizophrenia. *Psychol Med*. 2011;41(8):1709-1719. doi:10.1017/S003329171000156X

15. Samartzis L, Dima D, Fusar-Poli P, Kyriakopoulos M. White Matter Alterations in Early Stages of Schizophrenia: A Systematic Review of Diffusion Tensor Imaging Studies. *J Neuroimaging*. 2014;24(2):101-110. doi:10.1111/j.1552-6569.2012.00779.x

medRxiv preprint doi: https://doi.org/10.1101/2024.02.01.24301979; this version posted February 3, 2024. The copyright holder for this preprint (which was not certified by peer review) is the author/funder, who has granted medRxiv a license to display the preprint in perpetuity. All rights reserved. No reuse allowed without permission.

16. Tamnes CK, Agartz I. White Matter Microstructure in Early-Onset Schizophrenia: A Systematic Review of Diffusion Tensor Imaging Studies. *J Am Acad Child Adolesc Psychiatry*. 2016;55(4):269-279. doi:10.1016/j.jaac.2016.01.004

17. Kraguljac NV, McDonald WM, Widge AS, Rodriguez CI, Tohen M, Nemeroff CB. Neuroimaging Biomarkers in Schizophrenia. *Am J Psychiatry*. 2021;178(6):509-521. doi:10.1176/appi.ajp.2020.20030340

18. Sagarwala R, Nasrallah HA. The effect of antipsychotic medications on white matter integrity in first-episode drug-naïve patients with psychosis: A review of DTI studies. *Asian J Psychiatry*. 2021;61:102688. doi:10.1016/j.ajp.2021.102688

19. Lv J, Di Biase M, Cash RFH, Cocchi L, Cropley VL, Klauser P, et al. Individual deviations from normative models of brain structure in a large cross-sectional schizophrenia cohort. *Mol Psychiatry*. 2021;26(7):3512-3523. doi:10.1038/s41380-020-00882-5

20. Harrison PJ. The neuropathology of schizophrenia: A critical review of the data and their interpretation. *Brain*. 1999;122(4):593-624. doi:10.1093/brain/122.4.593

21. Hof PR, Haroutunian V, Friedrich VL, Byne W, Buitron C, Perl DP, et al. Loss and altered spatial distribution of oligodendrocytes in the superior frontal gyrus in schizophrenia. *Biol Psychiatry*. 2003;53(12):1075-1085. doi:10.1016/S0006-3223(03)00237-3

22. Uranova NA, Vikhreva OV, Rachmanova VI, Orlovskaya DD. Ultrastructural Alterations of Myelinated Fibers and Oligodendrocytes in the Prefrontal Cortex in Schizophrenia: A Postmortem Morphometric Study. *Schizophr Res Treat*. 2011;2011:e325789. doi:10.1155/2011/325789

23. Uranova NA, Vikhreva OV, Rakhmanova VI, Orlovskaya DD. Ultrastructural pathology of oligodendrocytes adjacent to microglia in prefrontal white matter in schizophrenia. *Npj Schizophr*. 2018;4(1):1-10. doi:10.1038/s41537-018-0068-2

24. Williams M, ed. *The Neuropathology of Schizophrenia*. Cham: Springer International Publishing; 2021. doi:10.1007/978-3-030-68308-5

25. Uranova NA, Vikhreva OV, Rakhmanova VI, Orlovskaya DD. Dystrophy of Oligodendrocytes and Adjacent Microglia in Prefrontal Gray Matter in Schizophrenia. *Front Psychiatry*. 2020;11. https://www.frontiersin.org/articles/10.3389/fpsyt.2020.00204. Accessed March 10, 2023.

26. Szeszko PR, Robinson DG, Ashtari M, Vogel J, Betensky J, Sevy S, et al. Clinical and Neuropsychological Correlates of White Matter Abnormalities in Recent Onset Schizophrenia. *Neuropsychopharmacology*. 2008;33(5):976-984. doi:10.1038/sj.npp.1301480

27. Peters BD, Karlsgodt KH. White matter development in the early stages of psychosis. *Schizophr Res*. 2015;161(1):61-69. doi:10.1016/j.schres.2014.05.021

28. Lang XE, Zhu D, Zhang G, Du X, Jia Q, Yin G, et al. Sex difference in association of symptoms and white matter deficits in first-episode and drug-naive schizophrenia. *Transl Psychiatry*. 2018;8(1):1-8. doi:10.1038/s41398-018-0346-9

29. Cai J, Xie M, Zhao L, Li X, Liang S, Deng W, et al. White matter changes and its relationship with clinical symptom in medication-naive first-episode early onset schizophrenia. *Asian J Psychiatry*. 2023;82:103482. doi:10.1016/j.ajp.2023.103482

30. Lodygensky GA, West T, Stump M, Holtzman DM, Inder TE, Neil JJ. In vivo MRI analysis of an inflammatory injury in the developing brain. *Brain Behav Immun*. 2010;24(5):759-767. doi:10.1016/j.bbi.2009.11.005

31. Guglielmetti C, Veraart J, Roelant E, Mai Z, Daans J, Van Audekerke J, et al. Diffusion kurtosis imaging probes cortical alterations and white matter pathology following cuprizone induced demyelination and spontaneous remyelination. *NeuroImage*. 2016;125:363-377. doi:10.1016/j.neuroimage.2015.10.052

32. Jelescu IO, Zurek M, Winters KV, Veraart J, Rajaratnam A, Kim NS, et al. In vivo quantification of demyelination and recovery using compartment-specific diffusion MRI metrics validated by electron microscopy. *NeuroImage*. 2016;132:104-114. doi:10.1016/j.neuroimage.2016.02.004

33. Winklewski PJ, Sabisz A, Naumczyk P, Jodzio K, Szurowska E, Szarmach A. Understanding the Physiopathology Behind Axial and Radial Diffusivity Changes-What Do We Know? *Front Neurol*. 2018;9:92. doi:10.3389/fneur.2018.00092

medRxiv preprint doi: https://doi.org/10.1101/2024.02.01.24301979; this version posted February 3, 2024. The copyright holder for this preprint (which was not certified by peer review) is the author/funder, who has granted medRxiv a license to display the preprint in perpetuity. All rights reserved. No reuse allowed without permission.

34. Jelescu IO, Fieremans E. Chapter 2 - Sensitivity and specificity of diffusion MRI to neuroinflammatory processes. In: Laule C, Port JD, eds. *Advances in Magnetic Resonance Technology and Applications*. Vol 9. Imaging Neuroinflammation. Academic Press; 2023:31-50. doi:10.1016/B978-0-323-91771-1.00010-1

35. Wijtenburg SA, Rowland LM. Chapter 19 - Schizophrenia spectrum disorders. In: Laule C, Port JD, eds. *Advances in Magnetic Resonance Technology and Applications*. Vol 9. Imaging Neuroinflammation. Academic Press; 2023:469-487. doi:10.1016/B978-0-323-91771-1.00008-3

36. Kubicki M, McCarley R, Westin CF, Park HJ, Maier S, Kikinis R, et al. A review of diffusion tensor imaging studies in schizophrenia. *J Psychiatr Res*. 2007;41(1):15-30. doi:10.1016/j.jpsychires.2005.05.005

37. Jensen JH, Helpern JA, Ramani A, Lu H, Kaczynski K. Diffusional kurtosis imaging: The quantification of non-gaussian water diffusion by means of magnetic resonance imaging. *Magn Reson Med*. 2005;53(6):1432-1440. doi:10.1002/mrm.20508

38. Jensen JH, Helpern JA. MRI quantification of non-Gaussian water diffusion by kurtosis analysis. *NMR Biomed*. 2010;23(7):698-710. doi:10.1002/nbm.1518

39. Narita H, Tha KK, Hashimoto N, Hamaguchi H, Nakagawa S, Shirato H, et al. Mean kurtosis alterations of cerebral white matter in patients with schizophrenia revealed by diffusion kurtosis imaging. *Prog Neuropsychopharmacol Biol Psychiatry*. 2016;71:169-175. doi:10.1016/j.pnpbp.2016.07.011

40. Zhu J, Zhuo C, Qin W, Wang D, Ma X, Zhou Y, et al. Performances of diffusion kurtosis imaging and diffusion tensor imaging in detecting white matter abnormality in schizophrenia. *NeuroImage Clin*. 2015;7:170-176. doi:10.1016/j.nicl.2014.12.008

41. Zhang F, Cho KIK, Tang Y, Zhang T, Kelly S, Biase MD, et al. MK-Curve improves sensitivity to identify white matter alterations in clinical high risk for psychosis. *NeuroImage*. 2021;226:117564. doi:10.1016/j.neuroimage.2020.117564

42. Jelescu IO, Budde MD. Design and Validation of Diffusion MRI Models of White Matter. *Front Phys*. 2017;5. https://www.frontiersin.org/articles/10.3389/fphy.2017.00061. Accessed December 1, 2022.

43. Pasternak O, Sochen N, Gur Y, Intrator N, Assaf Y. Free water elimination and mapping from diffusion MRI. *Magn Reson Med*. 2009;62(3):717-730. doi:10.1002/mrm.22055

44. Zhang H, Schneider T, Wheeler-Kingshott CA, Alexander DC. NODDI: practical in vivo neurite orientation dispersion and density imaging of the human brain. *NeuroImage*. 2012;61(4):1000-1016. doi:10.1016/j.neuroimage.2012.03.072

45. Carreira Figueiredo I, Borgan F, Pasternak O, Turkheimer FE, Howes OD. White-matter free-water diffusion MRI in schizophrenia: a systematic review and meta-analysis. *Neuropsychopharmacology*. 2022;47(7):1413-1420. doi:10.1038/s41386-022-01272-x

46. Cetin-Karayumak S, Lyall AE, Di Biase MA, Seitz-Holland J, Zhang F, Kelly S, et al. Characterization of the extracellular free water signal in schizophrenia using multi-site diffusion MRI harmonization. *Mol Psychiatry*. April 2023:1-9. doi:10.1038/s41380-023-02068-1

47. Rae CL, Davies G, Garfinkel SN, Gabel MC, Dowell NG, Cercignani M, et al. Deficits in Neurite Density Underlie White Matter Structure Abnormalities in First-Episode Psychosis. *Biol Psychiatry*. 2017;82(10):716-725. doi:10.1016/j.biopsych.2017.02.008

48. Kraguljac NV, Anthony T, Morgan CJ, Jindal RD, Burger MS, Lahti AC. White matter integrity, duration of untreated psychosis, and antipsychotic treatment response in medication-naïve first-episode psychosis patients. *Mol Psychiatry*. 2021;26(9):5347-5356. doi:10.1038/s41380-020-0765-x

49. Kraguljac NV, Anthony T, Monroe WS, Skidmore FM, Morgan CJ, White DM, et al. A longitudinal neurite and free water imaging study in patients with a schizophrenia spectrum disorder. *Neuropsychopharmacology*. 2019;44(11):1932-1939. doi:10.1038/s41386-019-0427-3

50. Jelescu IO, Veraart J, Fieremans E, Novikov DS. Degeneracy in model parameter estimation for multi-compartmental diffusion in neuronal tissue. *NMR Biomed*. 2016;29(1):33-47. doi:10.1002/nbm.3450

51. Jespersen SN, Olesen JL, Hansen B, Shemesh N. Diffusion time dependence of microstructural parameters in fixed spinal cord. *NeuroImage*. 2018;182:329-342. doi:10.1016/j.neuroimage.2017.08.039

medRxiv preprint doi: https://doi.org/10.1101/2024.02.01.24301979; this version posted February 3, 2024. The copyright holder for this preprint (which was not certified by peer review) is the author/funder, who has granted medRxiv a license to display the preprint in perpetuity. All rights reserved. No reuse allowed without permission.

52. Fieremans E, Jensen JH, Helpern JA. White matter characterization with diffusional kurtosis imaging. *NeuroImage*. 2011;58(1):177-188. doi:10.1016/j.neuroimage.2011.06.006

53. Diao Y, Jelescu I. Parameter estimation for WMTI-Watson model of white matter using encoder–decoder recurrent neural network. *Magn Reson Med*. 2023;89(3):1193-1206. doi:10.1002/mrm.29495

54. Kamiya K, Hori M, Irie R, Miyajima M, Nakajima M, Kamagata K, et al. Diffusion imaging of reversible and irreversible microstructural changes within the corticospinal tract in idiopathic normal pressure hydrocephalus. *NeuroImage Clin*. 2017;14:663-671. doi:10.1016/j.nicl.2017.03.003

55. de Kouchkovsky I, Fieremans E, Fleysher L, Herbert J, Grossman RI, Inglese M. Quantification of normal-appearing white matter tract integrity in multiple sclerosis: a diffusion kurtosis imaging study. *J Neurol*. 2016;263(6):1146-1155. doi:10.1007/s00415-016-8118-z

56. Benitez A, Fieremans E, Jensen JH, Falangola MF, Tabesh A, Ferris SH, et al. White matter tract integrity metrics reflect the vulnerability of late-myelinating tracts in Alzheimer's disease. *NeuroImage Clin*. 2014;4:64-71. doi:10.1016/j.nicl.2013.11.001

57. Dong JW, Jelescu IO, Ades-Aron B, Novikov DS, Friedman K, Babb JS, et al. Diffusion MRI biomarkers of white matter microstructure vary nonmonotonically with increasing cerebral amyloid deposition. *Neurobiol Aging*. 2020;89:118-128. doi:10.1016/j.neurobiolaging.2020.01.009

58. Tristão Pereira C, Diao Y, Yin T, da Silva AR, Lanz B, Pierzchala K, et al. Synchronous nonmonotonic changes in functional connectivity and white matter integrity in a rat model of sporadic Alzheimer's disease. *NeuroImage*. 2021;225:117498. doi:10.1016/j.neuroimage.2020.117498

59. Chung S, Fieremans E, Wang X, Kucukboyaci NE, Morton CJ, Babb J, et al. White Matter Tract Integrity: An Indicator of Axonal Pathology after Mild Traumatic Brain Injury. *J Neurotrauma*. 2018;35(8):1015-1020. doi:10.1089/neu.2017.5320

60. Yung AR, Yuen HP, McGorry PD, Phillips LJ, Kelly D, Dell'Olio M, et al. Mapping the onset of psychosis: the Comprehensive Assessment of At-Risk Mental States. *Aust N Z J Psychiatry*. 2005;39(11-12):964-971. doi:10.1080/j.1440-1614.2005.01714.x

61. Tustison NJ, Avants BB, Cook PA, Zheng Y, Egan A, Yushkevich PA, et al. N4ITK: improved N3 bias correction. *IEEE Trans Med Imaging*. 2010;29(6):1310-1320. doi:10.1109/TMI.2010.2046908

62. Grabner G, Janke AL, Budge MM, Smith D, Pruessner J, Collins DL. Symmetric Atlasing and Model Based Segmentation: An Application to the Hippocampus in Older Adults. In: Larsen R, Nielsen M, Sporring J, eds. *Medical Image Computing and Computer-Assisted Intervention – MICCAI 2006*. Lecture Notes in Computer Science. Berlin, Heidelberg: Springer; 2006:58-66. doi:10.1007/11866763_8

63. Avants BB, Epstein CL, Grossman M, Gee JC. Symmetric diffeomorphic image registration with cross-correlation: evaluating automated labeling of elderly and neurodegenerative brain. *Med Image Anal*. 2008;12(1):26-41. doi:10.1016/j.media.2007.06.004

64. Ades-Aron B, Veraart J, Kochunov P, McGuire S, Sherman P, Kellner E, et al. Evaluation of the accuracy and precision of the diffusion parameter EStImation with Gibbs and NoisE removal pipeline. *NeuroImage*. 2018;183:532-543. doi:10.1016/j.neuroimage.2018.07.066

65. Veraart J, Sijbers J, Sunaert S, Leemans A, Jeurissen B. Weighted linear least squares estimation of diffusion MRI parameters: Strengths, limitations, and pitfalls. *NeuroImage*. 2013;81:335-346. doi:10.1016/j.neuroimage.2013.05.028

66. Mori S, Wakana S, Van Zijl PC, Nagae-Poetscher LM. *MRI Atlas of Human White Matter*. Elsevier; 2005.

67. American Psychiatric Association. *Diagnostic and Statistical Manual of Mental Disorders (4th Ed., Text Rev.)*.; 2000.

68. Kay SR, Fiszbein A, Opler LA. The Positive and Negative Syndrome Scale (PANSS) for Schizophrenia. *Schizophr Bull*. 1987;13(2):261-276. doi:10.1093/schbul/13.2.261

69. Montgomery SA, Asberg M. A new depression scale designed to be sensitive to change. *Br J Psychiatry J Ment Sci*. 1979;134:382-389. doi:10.1192/bjp.134.4.382

medRxiv preprint doi: https://doi.org/10.1101/2024.02.01.24301979; this version posted February 3, 2024. The copyright holder for this preprint (which was not certified by peer review) is the author/funder, who has granted medRxiv a license to display the preprint in perpetuity. All rights reserved. No reuse allowed without permission.

70. Young RC, Biggs JT, Ziegler VE, Meyer DA. A Rating Scale for Mania: Reliability, Validity and Sensitivity. *Br J Psychiatry*. 1978;133(5):429-435. doi:10.1192/bjp.133.5.429

71. Wallwork RS, Fortgang R, Hashimoto R, Weinberger DR, Dickinson D. Searching for a consensus five-factor model of the Positive and Negative Syndrome Scale for schizophrenia. *Schizophr Res*. 2012;137(1-3):246-250. doi:10.1016/j.schres.2012.01.031

72. Fortin JP, Parker D, Tunç B, Watanabe T, Elliott MA, Ruparel K, et al. Harmonization of multi-site diffusion tensor imaging data. *NeuroImage*. 2017;161:149-170. doi:10.1016/j.neuroimage.2017.08.047

73. Alemán-Gómez Y, Najdenovska E, Roine T, Fartaria MJ, Canales-Rodríguez EJ, Rovó Z, et al. Partial-volume modeling reveals reduced gray matter in specific thalamic nuclei early in the time course of psychosis and chronic schizophrenia. *Hum Brain Mapp*. 2020;41(14):4041-4061. doi:10.1002/hbm.25108

74. Shapiro SS, Wilk MB. An analysis of variance test for normality (complete samples)†. *Biometrika*. 1965;52(3-4):591-611. doi:10.1093/biomet/52.3-4.591

75. Zimmerman DW. A note on preliminary tests of equality of variances. *Br J Math Stat Psychol*. 2004;57(1):173-181. doi:10.1348/000711004849222

76. Wilcoxon F. Individual Comparisons by Ranking Methods. *Biom Bull*. 1945;1(6):80-83. doi:10.2307/3001968

77. Brunner E, Munzel U. The Nonparametric Behrens-Fisher Problem: Asymptotic Theory and a Small-Sample Approximation. *Biom J*. 2000;42(1):17-25. doi:10.1002/(SICI)1521-4036(200001)42:1<17::AID-BIMJ17>3.0.CO;2-U

78. Karch JD. Psychologists Should Use Brunner-Munzel's Instead of Mann-Whitney's U Test as the Default Nonparametric Procedure. *Adv Methods Pract Psychol Sci*. 2021;4(2):2515245921999602. doi:10.1177/2515245921999602

79. R Core Team. *R: A Language and Environment for Statistical Computing*. Vienna, Austria: R Foundation for Statistical Computing; 2023. https://www.R-project.org/.

80. Maechler M, Rousseeuw P, Croux C, Todorov V, Ruckstuhl A, Salibian-Barrera M, et al. *Robustbase: Basic Robust Statistics.*; 2023. http://robustbase.r-forge.r-project.org/.

81. Todorov V, Filzmoser P. An Object-Oriented Framework for Robust Multivariate Analysis. *J Stat Softw*. 2009;32(3):1-47.

82. Hatton SN, Lagopoulos J, Hermens DF, Hickie IB, Scott E, Bennett MR. White matter tractography in early psychosis: clinical and neurocognitive associations. *J Psychiatry Neurosci*. 2014;39(6):417-427. doi:10.1503/jpn.130280

83. Kraguljac NV, Guerreri M, Strickland MJ, Zhang H. Neurite Orientation Dispersion and Density Imaging in Psychiatric Disorders: A Systematic Literature Review and a Technical Note. *Biol Psychiatry Glob Open Sci*. 2023;3(1):10-21. doi:10.1016/j.bpsgos.2021.12.012

84. Kitamura H, Matsuzawa H, Shioiri T, Someya T, Kwee IL, Nakada T. Diffusion tensor analysis in chronic schizophrenia A preliminary study on a high–field (3.0T) system. *Eur Arch Psychiatry Clin Neurosci*. 2005;255(5):313-318. doi:10.1007/s00406-005-0564-z

85. Sato Y, Sakuma A, Ohmuro N, Katsura M, Abe K, Tomimoto K, et al. Relationship Between White Matter Microstructure and Hallucination Severity in the Early Stages of Psychosis: A Diffusion Tensor Imaging Study. *Schizophr Bull Open*. 2021;2(1):sgab015. doi:10.1093/schizbullopen/sgab015

86. Wu EX, Cheung MM. MR diffusion kurtosis imaging for neural tissue characterization. *NMR Biomed*. 2010;23(7):836-848. doi:10.1002/nbm.1506

87. Pasternak O, Kelly S, Sydnor VJ, Shenton ME. Advances in microstructural diffusion neuroimaging for psychiatric disorders. *NeuroImage*. 2018;182:259-282. doi:10.1016/j.neuroimage.2018.04.051

88. Abdul-Rahman MF, Qiu A, Sim K. Regionally Specific White Matter Disruptions of Fornix and Cingulum in Schizophrenia. *PLOS ONE*. 2011;6(4):e18652. doi:10.1371/journal.pone.0018652

medRxiv preprint doi: https://doi.org/10.1101/2024.02.01.24301979; this version posted February 3, 2024. The copyright holder for this preprint (which was not certified by peer review) is the author/funder, who has granted medRxiv a license to display the preprint in perpetuity. All rights reserved. No reuse allowed without permission.

89. Luck D, Malla AK, Joober R, Lepage M. Disrupted integrity of the fornix in first-episode schizophrenia. *Schizophr Res*. 2010;119(1):61-64. doi:10.1016/j.schres.2010.03.027

90. Koshiyama D, Fukunaga M, Okada N, Morita K, Nemoto K, Yamashita F, et al. Role of frontal white matter and corpus callosum on social function in schizophrenia. *Schizophr Res*. 2018;202:180-187. doi:10.1016/j.schres.2018.07.009

91. Chen S, Tang Y, Fan X, Qiao Y, Wang J, Wen H, et al. The role of white matter abnormality in the left anterior corona radiata: In relation to formal thought disorder in patients with schizophrenia. *Psychiatry Res*. 2022;307:114302. doi:10.1016/j.psychres.2021.114302

92. Meng L, Li K, Li W, Xiao Y, Lui S, Sweeney JA, et al. Widespread white-matter microstructure integrity reduction in first-episode schizophrenia patients after acute antipsychotic treatment. *Schizophr Res*. 2019;204:238-244. doi:10.1016/j.schres.2018.08.021

93. Ochi R, Noda Y, Tsuchimoto S, Tarumi R, Honda S, Matsushita K, et al. White matter microstructural organizations in patients with severe treatment-resistant schizophrenia: A diffusion tensor imaging study. *Prog Neuropsychopharmacol Biol Psychiatry*. 2020;100:109871. doi:10.1016/j.pnpbp.2020.109871

94. Elfaki AA, Elfaki A, Osman T, Sahin B, Elsheikh A, Mohamed A, et al. STEREOLOGICAL EVALUATION OF BRAIN MAGNETIC RESONANCE IMAGES OF SCHIZOPHRENIC PATIENTS. *Image Anal Stereol*. 2013;32(3):145-153. doi:10.5566/ias.v32.p145-153

95. Dunleavy C, Elsworthy RJ, Upthegrove R, Wood SJ, Aldred S. Inflammation in first-episode psychosis: The contribution of inflammatory biomarkers to the emergence of negative symptoms, a systematic review and meta-analysis. *Acta Psychiatr Scand*. 2022;146(1):6-20. doi:10.1111/acps.13416

96. Goldsmith DR, Rapaport MH, Miller BJ. A meta-analysis of blood cytokine network alterations in psychiatric patients: comparisons between schizophrenia, bipolar disorder and depression. *Mol Psychiatry*. 2016;21(12):1696-1709. doi:10.1038/mp.2016.3

97. Arrasate M, González-Ortega I, García-Alocén A, Alberich S, Zorrilla I, González-Pinto A. Prognostic Value of Affective Symptoms in First-Admission Psychotic Patients. *Int J Mol Sci*. 2016;17(7):1039. doi:10.3390/ijms17071039

98. Sönmez N, Røssberg JI, Evensen J, Barder HE, Haahr U, ten Velden Hegelstad W, et al. Depressive symptoms in first-episode psychosis: a 10-year follow-up study. *Early Interv Psychiatry*. 2016;10(3):227-233. doi:10.1111/eip.12163

99. He E, Liu M, Gong S, Fu X, Han Y, Deng F. White Matter Alterations in Depressive Disorder. *Front Immunol*. 2022;13:826812. doi:10.3389/fimmu.2022.826812

100. Bopp MHA, Zöllner R, Jansen A, Dietsche B, Krug A, Kircher TTJ. White matter integrity and symptom dimensions of schizophrenia: A diffusion tensor imaging study. *Schizophr Res*. 2017;184:59-68. doi:10.1016/j.schres.2016.11.045

101. Vignapiano A, Koenig T, Mucci A, Giordano GM, Amodio A, Altamura M, et al. Disorganization and cognitive impairment in schizophrenia: New insights from electrophysiological findings. *Int J Psychophysiol*. 2019;145:99-108. doi:10.1016/j.ijpsycho.2019.03.008

102. Najjar S, Pearlman DM. Neuroinflammation and white matter pathology in schizophrenia: systematic review. *Schizophr Res*. 2015;161(1):102-112. doi:10.1016/j.schres.2014.04.041

103. Hoptman MJ, Volavka J, Johnson G, Weiss E, Bilder RM, Lim KO. Frontal white matter microstructure, aggression, and impulsivity in men with schizophrenia: a preliminary study. *Biol Psychiatry*. 2002;52(1):9-14. doi:10.1016/S0006-3223(02)01311-2

104. Nishimura Y, Takizawa R, Muroi M, Marumo K, Kinou M, Kasai K. Prefrontal cortex activity during response inhibition associated with excitement symptoms in schizophrenia. *Brain Res*. 2011;1370:194-203. doi:10.1016/j.brainres.2010.11.003